

The gravitational and hydrodynamical interaction between the LMC and the Galaxy

C. Mastropietro,^{1*} B. Moore¹, L. Mayer¹, J. Wadsley² and J. Stadel¹

¹*Institute for Theoretical Physics, University of Zürich, CH-8057 Zürich, Switzerland*

²*Department of Physics & Astronomy, McMaster University, 1280 Main St. West, Hamilton ON L8S 4M1 Canada*

25 June 2018

ABSTRACT

We use high resolution N-Body/SPH simulations to study the hydrodynamical and gravitational interaction between the Large Magellanic Cloud and the Milky Way. We model the dark and hot extended halo components as well as the stellar/gaseous disks of the two galaxies. Both galaxies are embedded in extended cuspy LCDM dark matter halos. We follow the previous four Gyrs of the LMC’s orbit such that it ends up with the correct location and orientation on the sky. Tidal forces elongate the LMC’s disk, forcing a bar and creating a strong warp and diffuse stellar halo, although very few stars become unbound. The stellar halo may account for some of the microlensing events. Ram-pressure from a low density ionised halo is then sufficient to remove $1.4 \times 10^8 M_{\odot}$ of gas from the LMC’s disk forming a great circle trailing stream around the Galaxy. The column density of stripped gas falls by two orders of magnitude 100 degrees from LMC. The LMC does not induce any response in the Milky Way disk. On the contrary, the tides raised by the Milky Way determine the truncation of the satellite at about 11 kpc. After several Gyrs of interaction the gas disk of the LMC is smaller than the stellar disk due to ram pressure and its size compares well with the observational data.

Key words: methods: N-body simulations – galaxies: Magellanic Clouds – galaxies: interactions – hydrodynamics

1 INTRODUCTION

The Large Magellanic Cloud (LMC) is in the process of destroying its neighbour, the Small Magellanic Cloud (SMC). In turn, the Milky Way (MW) is playing a role reshaping these galaxies and creating the spectacular Magellanic Stream (hereafter MS). The MS is a trailing filament of neutral hydrogen that originates from the Magellanic Clouds and stretches for over ~ 100 degrees in the Southern Sky and is the most prominent signature of an interaction between the Clouds and the Milky Way. The combined interaction between these three galaxies must strongly influence the morphological evolution of the Clouds, as well as their internal kinematics and star formation history. A resonant interaction between the Galaxy and the LMC could even be sufficient to excite the warp observed in the Galactic disk (Weinberg 1995, 1998).

Several models have been proposed in order to study the nature of this interaction and to isolate the main mechanism responsible for the formation of the Stream. These models

have become increasingly refined over the years. The first gravitational tidal models took into account just the binary interaction between the LMC and MW (Lin & Lynden-Bell 1977; Murai & Fujimoto 1980), but later models included a close interaction between the Clouds themselves during a previous passage at the perigalacticon about 1.5 Gyrs ago (Gardiner, Sawa, & Fujimoto 1994; Lin, Jones, & Klemola 1995; Gardiner & Noguchi 1996).

The strongest argument which supports a tidal origin for the MS is provided by the discovery of neutral hydrogen in front of the LMC (Putman et al. 1998). However the amount of material in this feature is just a fraction of the mass of the MS (Putman et al. 2003a). However there are some characteristics of the Stream that tidal models cannot explain. In particular they fail in reproducing the gradual decrease of the HI column density and the lack of a stellar tidal feature (Mathewson et al. 1979; Brueck & Hawkins 1983; Guhathakurta & Reitzel 1998). Stars are expected to be stripped by gravitational forces along with the gas, although Weinberg (2000) suggests that the stellar debris would have a different distribution respect to the gaseous Stream and form a diffuse envelope around the LMC. Traces of an offset old stellar stream could be identified with the

* E-mail: chiara@physik.unizh.ch

giant stars observed by Majewski et al. (1999) around the Magellanic Clouds.

A hydrodynamical interaction has also been invoked to explain the Stream. Mathewson et al. (1987) proposed that gas is swept away from the intra-cloud region and decelerated by random collisions with high velocity clouds (HVC). This model requires unrealistic densities for the HVCs in the MW halo in order to justify the high number of encounters that should generate the Stream and does not explain the column density gradient. Continuous stripping models (Meurer, Bicknell & Gingold 1985; Sofue 1994; Moore & Davis 1994) propose a scenario in which gas is stripped by ram-pressure forces from the outer regions of the Clouds through an interaction with a distribution of hot gas in the halo or an extended ionised disk. A satellite moving with a relative velocity v respect to this external medium of density ρ experiences a pressure $P = \rho v^2$ which can be sufficient to remove part of the neutral gas from the disk.

Together with the difficulties in creating a continuous leading arm – although the stripped material decelerated by ram pressure forces could fall on smaller orbits and lead the Clouds (Sofue 1994; Moore & Davis 1994) – ram pressure models are thought to be able to reproduce the large amount of gas observed in the Stream ($\sim 2 \times 10^8 M_\odot$ according to Putman et al. 2003a).

The presence of an extended hot halo surrounding the MW and in hydrostatic equilibrium within the dark matter potential is expected by current models of hierarchical structure formation (White & Frenk 1991). This gaseous halo, left over from the initial collapse, would be continuously fuelled by accretion of satellite galaxies over time. Recent observational results have confirmed the existence of a distribution of hot ($T \sim 10^6$ K) gas well beyond the Galactic disk, with a radius larger than 70 kpc in order to explain some ionisation features discovered in the MS (Sembach et al 2003; Putman et al. 2003b). Constraints from dynamical and thermal arguments fix the density of the gaseous halo in a range between 10^{-5} and 10^{-4}cm^{-3} at the LMC distance from the Galactic center. The Clouds are therefore subjected along their orbits to the ram pressure generated by a tenuous distribution of hot gas and the Magellanic System itself seems to be the result of a complex interaction that involves both hydrodynamical and tidal processes.

The aim of this work is to study for the first time the simultaneous effect of gravitational and hydrodynamical forces acting on the LMC as it moves within the Galactic halo, using fully self consistent galaxy models. In particular we are interested in the formation and evolution of the Magellanic Stream and in the dynamical changes in the internal structure of the LMC due to the interaction with the MW. We ignore the SMC owing to its small mass ($\sim 10\%$ of the LMC), neglecting the possibility of a close encounter between the two Clouds and the consequence of additional loss of mass. This approximation would lead to an underestimation of the amount of HI in the Stream.

This paper is structured as follows. In Section 2 we present the main characteristics of the galaxy models that we use. The results of test wind tube simulations are dis-

Table 1. Galaxy models: for each component mass (in units of $10^{10} M_\odot$ and scale radius (kpc) are indicated. The last three columns refer to high resolution runs and report number of particles, mass particle (in units of $10^5 M_\odot$) and softening length (kpc).

| MW | Mass | Scale radius | N | m | ϵ |
|--------------|-------|--------------|-----------------|------|------------|
| Bulge | 0.73 | 0.70 | 10^4 | 7.3 | 0.1 |
| Gaseous disk | 0.46 | 3.53 | 10^5 | 0.46 | 0.1 |
| Stellar disk | 4.10 | 3.53 | 10^5 | 4.10 | 0.1 |
| DM halo | 104.0 | 18.2 | 10^6 | 10.4 | 0.5 |
| Hot halo | 1.0 | 18.2 | 5×10^5 | 0.20 | 0.5 |
| LMC | Mass | Scale radius | N | m | ϵ |
| Gaseous disk | 0.11 | 1.66 | 10^5 | 0.11 | 0.1 |
| Stellar disk | 0.11 | 1.66 | 5×10^4 | 0.22 | 0.1 |
| DM halo | 2.38 | 6.02 | 6×10^5 | 10.4 | 0.5 |

cussed in Section 3. In Section 4 we analyse the results of the interacting runs regarding the Stream and the LMC disk.

2 GALAXY MODELS

The initial conditions of the simulations are constructed using the technique described by Hernquist (1993). Both the Milky Way and the Large Magellanic Cloud are multi-component systems with a stellar and gaseous disk embedded in a spherical dark matter halo. The density profile of the NFW (Navarro, Frenk & White 1997) halo is adiabatically contracted due to baryonic cooling (Springel & White 1999). Stars and cold ($T = 10^4$ K) gas in the disk follow the same exponential surface density profile of the form

$$\Sigma(R) = \frac{M_d}{2\pi R_d^2} \exp(-R/R_d), \quad (1)$$

where M_d and R_d are the disk mass and radial scale length (in cylindrical coordinates) respectively, while the thin vertical structure is characterised by the scale height $z_d \sim \frac{1}{5} R_d$:

$$\rho_d(R, z) = \frac{\Sigma(R)}{2z_d} \text{sech}^2(z/z_d). \quad (2)$$

The MW model comprises of two further components: a stellar bulge and an extended hot gaseous halo. The bulge has a spherical Hernquist (Hernquist 1990) profile:

$$\rho_b(r) = \frac{M_b}{2\pi} \frac{r_b}{r(r_b + r)^3} \quad (3)$$

where M_b is the bulge mass and r_b its scale length.

Although the presence of an extended corona of hot gas seems to be the most likely explanation for the detection of OVI and OVII absorption lines associated with HI structures (MS, some HVCs, Outer Spiral Arm, Complex A, Complex C, according to Sembach et al. 2003), its density structure is still uncertain, particularly at large distances from the Galactic center. These ionization features suggest a mean density of the gaseous halo within 80 kpc of $\sim 10^{-4} - 10^{-5} \text{cm}^{-3}$ (Sembach 2003). Stanimirovic (2002) provides similar values for the density at 45 kpc ($n_h \lesssim 3 \times 10^{-4} \text{cm}^{-3}$) in order to explain the confinement mechanism of the MS clouds through pressure support from the hot halo. Another constraint comes from the detection of

$H\alpha$ emission along the MS which cannot be explained solely by photoionisation from the Galactic disk (Putman et al. 2003b) and could be induced by the interaction with a relative dense ($n_h > 10^{-4}\text{cm}^{-3}$ at 50 kpc) gaseous environment (Weiner & Williams 1996). With a density higher than 10^{-4}cm^{-3} Quilis & Moore (2001) are able to reproduce, using hydrodynamical simulations, the head-tail structure and the compression fronts associated with HVCs, in the case of either pure gas clouds or gas embedded within a dark matter halo. A significantly lower value for the upper limit of the halo density ($n_h < 10^{-5}\text{cm}^{-3}$) is found by Murali (2000) by requiring the survival of the cloud MS IV for 500 Myrs against evaporation. However we emphasise the fact that the evaporation time strongly depends on the temperature of the gaseous halo (Cowie & McKee 1977) and a choice of $T \sim 10^6\text{K}$, three times lower than the value used by Murali, increases by almost a factor fifteen the lifetime of MS IV, making the survival of the cloud possible at a density of even 10^{-4}cm^{-3} . At larger distances from the Galactic center constraints on the halo density are poor, although Blitz & Robishaw (2000) derive a value of $2.5 \times 10^{-5}\text{cm}^{-3}$ at a distance of 200 kpc by applying ram pressure stripping to dwarf spheroidal galaxies within the Galactic halo.

We model the hot halo with a spherical distribution of gas which traces the dark matter profile within the virial radius and is in hydrostatical equilibrium inside the Galactic potential. Assuming an isotropic model, the halo temperature at a given radius r is determined by the cumulative mass distribution $M(r)$ of the dark, stellar and gaseous components of the MW beyond r and by the density profile $\rho_h(r)$ of the hot gas:

$$T(r) = \frac{m_p}{k_B} \frac{1}{\rho_h(r)} \int_r^\infty \rho_h(r) \frac{GM(r)}{r^2} dr, \quad (4)$$

where m_p is the proton mass, G and k_B are the gravitational and Boltzmann constants. The halo gas is completely ionised at a mean temperature of 10^6K . We normalise the density profile using a hot halo mass of $M_h = 10^{10}M_\odot$, which corresponds to a mean density of $2 \times 10^{-5}\text{cm}^{-3}$ within 150 kpc and 8.5×10^{-5} at 50 kpc. With the assumption that the gas traces the dark matter we overestimate by a factor of three the ionised gas density near the disk, however this is not important for the current study.

The masses and the scale lengths of the MW and LMC models (Table 1) are selected in order to reproduce observational constraints from Kim et al. (1998) and van der Marel et al. (2002), while for the MW we adopt a model similar to model A_1 of Klypin, Zhao & Somerville (2002). Fig. 1 and Fig. 2 show the rotation curves of the different components of the two galaxies. The concentration c and the spin parameter λ (Mo, Mao & White 1998) are indicated at the top left. The concentration is defined as $cc = r_{vir}/r_s$, where r_{vir} and r_s are the virial and the scale radius of the NFW halo, whereas the spin parameter relates the angular momentum J and the total energy E of an halo with a virial mass M_{vir} through the relation $\lambda = J|E|^{1/2}G^{-1}M_{vir}^{-5/2}$. The disk of the satellite galaxy has, within the scale radius, a central mass surface density of $\sim 70 M_\odot\text{pc}^{-2}$, which corresponds to a B-band surface brightness of $\sim 23\text{mag arcsec}^{-2}$, if we adopt a mass to light ratio of two.

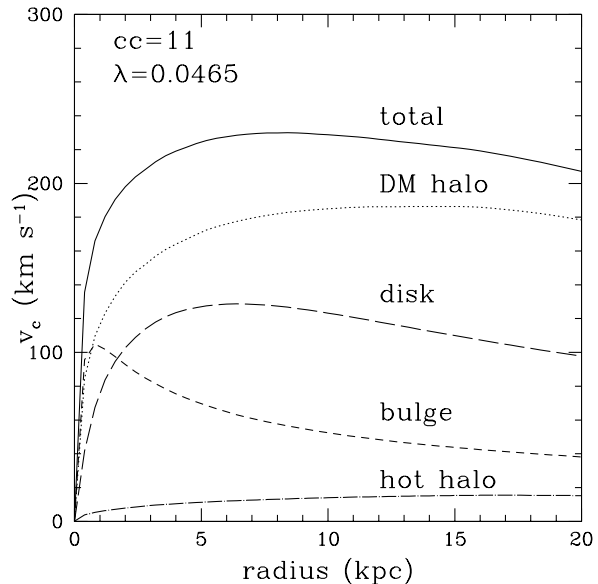


Figure 1. MW rotation curves. On the top left spin and concentration parameter are indicated.

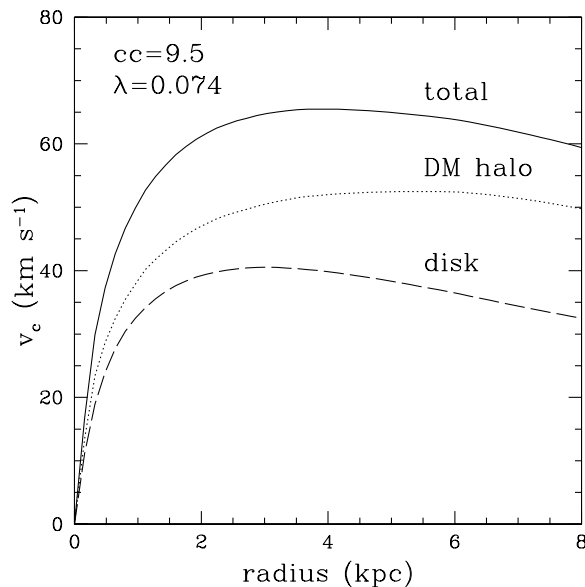


Figure 2. LMC rotation curves. On the top left spin and concentration parameter are indicated.

The thickness of the disks is set such that Toomre's (Toomre 1964) stability criterion is satisfied, which requires, for a stellar disk

$$Q_{star}(r) = \frac{\sigma_R k}{3.36 G \Sigma_s} > 1, \quad (5)$$

where σ_R is the radial velocity dispersion, k is the local epicyclic frequency and Σ_s the stellar surface density. For a gaseous disk Equation 5 becomes:

$$Q_{gas}(r) = \frac{v_s k}{\pi G \Sigma_g} > 1, \quad (6)$$

where v_s is the sound velocity and Σ_g the surface density of the gas.

All the simulations we now discuss were carried out using GASOLINE, a parallel tree-code with multi-stepping (Wadsley, Stadel & Quinn 2004). The high resolution runs have 2.46×10^6 particles, of which 3.5×10^5 are used for the disks and 5×10^5 for the hot halo of the MW (Table 1). The gravitational spline softening is set equal to 0.5 kpc for the dark and gaseous halos, and to 0.1 kpc for stars and gas in the disk and bulge components.

3 TEST SIMULATIONS

The mass resolution of the simulations strongly influences the ram pressure process. In particular, if the particles of the hot external medium are too massive, they do not flow smoothly on to the disk, but produce scattering and numerical holes, increasing the stripping process which is dominated by noise. In order to study these effects, we perform several test simulations in which we place the model LMC galaxy within a “wind tunnel” and vary the mass of the hot halo particles for a fixed resolution of the LMC disk.

The first set (H1, H2 and H3) of runs simulates the passage of the satellite at the perigalacticon, which is the point along the orbit where ram pressure is most efficient due to the high values of ρ_g and v . The volume of the simulations is an oblong of base equal to the diameter of the LMC and height $h = vt$, where v is the velocity of the satellite at the perigalacticon (250 km s^{-1}) and t is set ~ 2 Gyrs (\sim the inferred orbital time for the LMC). We represent the hot gas as a flux of particles moving with a velocity v along the z axis, parallel to the angular momentum of the disk. The hot particles have an initial random distribution, a temperature $T = 10^6 \text{ K}$ and a number density $n_h = 8 \times 10^{-5} \text{ cm}^{-3}$. The box has periodic boundary conditions in order to restore the flow of hot gas that leaves the oblong. The disk particles have the same mass m_{disk} as in the high resolution interacting runs (see Table 2), while the mass ratio with the particles in the oblong m_h/m_{disk} of 1:10, 1:2 and 1:1. Gas is removed from the disk if the ram pressure produced by the hot halo of the MW is greater than the restoring force per unit area provided by the disk of the satellite. The condition for ram pressure stripping is expressed by (Gunn & Gott 1972)

$$\rho_h v^2 > 2\pi G \Sigma(R) \Sigma_g(R), \quad (7)$$

where v is the velocity of the galaxy with respect to the surrounding medium, ρ_h is the density of the hot halo of the MW and $\Sigma_g(r)$ is the cold gas surface density at the radius R . Σ represents the gravitational surface mass density of the disk. The minimum radius given by Equation (7) is the final stripping radius R_{str} beyond which the ISM can be removed from the galaxy. The halo component does not contribute to the restoring force initially, since in the case of a face on impact any force associated to a spherical potential is perpendicular to the wind pressure. As the gas is stripped out from the disk in the z direction, the disk gravity decreases while the projection of the radial halo gravity force in the z direction rises (Schulz & Struck 2001). This effect is particularly important in the case of low ram pressure regimes as the ones we are interested in here. The condition

for stripping expressed in Equation (7) implicitly assumes instantaneous stripping from the disk and discrete ram pressure stripping events such that the loss of mass approaches an asymptotic limit. If instead ram pressure is a continuous process with time scales comparable with the orbital time of the satellite, the stripping radius calculated analytically underestimates the physical size of the gaseous disk. Such a continuous ram pressure stripping occurs here not because of turbulent or viscous stripping but because the gas at the edge of the disk heats up responding to the compression exerted by the outer medium and can therefore become unbound by increasing its energy despite the ram pressure wind being constant. Timescales of both Kelvin-Helmoltz instabilities and artificial viscous forces are close to 10 Gyr because of, respectively, stabilization due to the cuspy halo potential of the LMC and the high mass resolution employed, and are therefore negligible over the timescales explored here.

We estimate R_{str} as the radius which contains 99% of the gas particles in the midplane of the disk. The mass of gas that remains in the disk can be computed summing the disk particles inside a cylinder of radius R_{str} and thickness 1 kpc. The mass of gas bound to the satellite at a time t is instead not directly related to R_{str} , but is determined by the potential of the dark halo. We calculate it balancing kinetic, thermal and potential energy in concentric spherical shells centered on the LMC, defining the gas tidal radius r_g as the radius of the most distant bound shell.

The mass of cold gas stripped from the LMC’s disk m_{str} decreases as we decrease the mass of the halo particles: in H1 m_{str} is ~ 1.6 times larger than in H3 (Table 2). Mass resolution also determinates the shape of the front edge and influences the morphology of the gaseous disk. Fig. 3 shows the gas density in the disk after 2 Gyrs for the H1, H2 and H3 runs. Numerical effects in the low resolution run are quite evident: the massive hot particles produce particle – particle interactions with gas in the galaxy, creating holes and discontinuities along the front edge of the disk. The spiral pattern is partially destroyed and the disk loses its symmetry. Scattering reduces the stripping radius by a factor of 1.4 and produces a sharp truncation, while the effect of pure ram pressure is much more gradual, since halo particles stream around the disk. Finally, the removed gas forms an asymmetric and turbulent tail. The high resolution H3 run appears very symmetric with a flat and uniform edge and a regular stream, which flows around the disk and creates a low density region behind (Fig. 4). As previously noticed by several authors (Quilis, Moore & Bower 2000; Quilis & Moore 2001; Schulz & Struck 2001), a bow shock forms in front of the disk, increasing the local ICM temperature from 10^6 to 2.5×10^6 degrees. The intermediate run H2 is similar to H1, although the gas tail is more pronounced and the amount of stripped gas is less than 10% larger. The resolution (mass ratio of 1:2) of the H2 run is to be a good compromise between the necessity of solving the gas dynamics and the number of particles to use in a full production simulation.

The runs L1, L2 and L3 have a gas density ($\rho_h = 3.5 \times 10^{-5} \text{ cm}^{-3}$) and satellite velocity (175 km s^{-1}) similar to our final LMC’s orbit with apocentric distance ~ 50 kpc and apo/peri ratio $\sim 2.5 : 1$ (see section 4.1). Reducing the ram pressure by a factor of three decreases the stripped mass by $\sim 20\%$, while the amount of unbound gas is almost 60% smaller. This indicates that a lower ram pressure

Table 2. LMC wind tunnel simulations. For each run the density ρ_h of the hot medium and the velocity v of the satellite are indicated. The resolution of each model is expressed in terms of the mass ratio m_h/m_{disk} between halo and disk particles. N is the number of hot particles, while the last four columns give the ram pressure stripping radius R_{str} and the mass stripped from the disk m_{str} , the gas tidal radius r_g and the mass of gas unbound to the galaxy m_{unb} . In the case of edge on galaxies the stripping radius R_{str} is the average value between the two sides of the disk. All the values are calculated at $t = 2$ Gyrs.

| Run | Model | ρ_g (10^{-5}cm^{-3}) | v (km s^{-1}) | m_h/m_{disk} | N (10^6) | R_{str} (kpc) | m_{str} ($10^8 M_\odot$) | r_g (kpc) | m_{unb} ($10^8 M_\odot$) |
|-----|---------|---|-------------------------------|----------------|-------------------|--------------------|---------------------------------|----------------|---------------------------------|
| H1 | face on | 8 | 250 | 10 | 0.37 | 4.0 | 4.11 | 6.7 | 2.84 |
| H2 | face on | 8 | 250 | 2 | 1.86 | 5.3 | 2.76 | 7.5 | 1.32 |
| H3 | face on | 8 | 250 | 1 | 3.2 | 5.5 | 2.52 | 7.8 | 1.0 |
| L1 | face on | 3.5 | 175 | 2 | 0.54 | 6.6 | 2.09 | 8.3 | 0.58 |
| L2 | face on | 3.5 | 175 | 1 | 1.07 | 6.8 | 2.02 | 8.5 | 0.44 |
| L3 | face on | 3.5 | 175 | 0.5 | 2.14 | 6.9 | 1.99 | 8.6 | 0.42 |
| E1 | edge on | 8 | 250 | 2 | 1.86 | 5.5 | 2.74 | 7.7 | 1.32 |
| E2 | edge on | 3.5 | 175 | 2 | 1.07 | 6.2 | 2.32 | 8.1 | 0.79 |

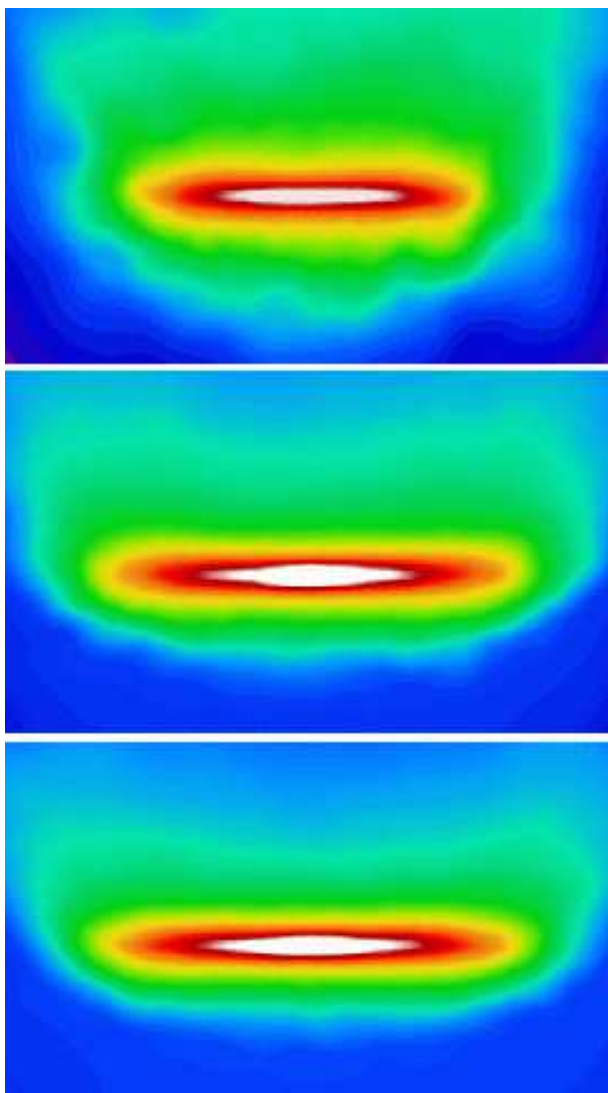


Figure 3. From the top to the bottom: column density distribution for the LMC test models H1, H2, H3. The scale is logarithmic with blue corresponding to the density of the hot halo gas.

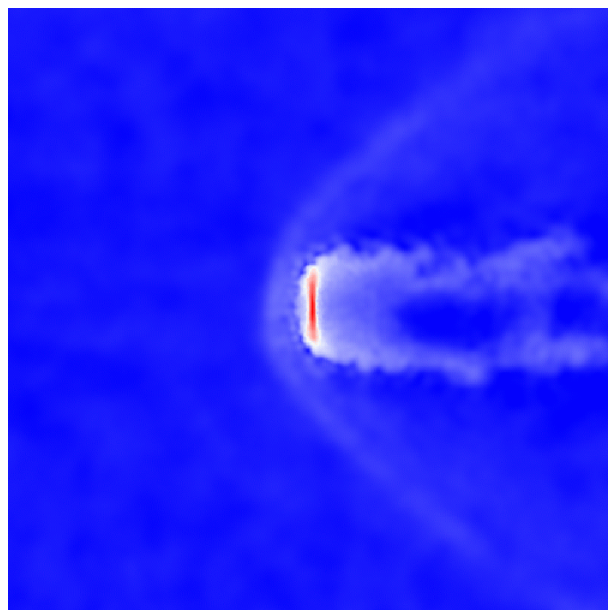


Figure 4. H3 run: density distribution of gas in a thin slice perpendicular to the LMC disk. The satellite is moving face on toward the left side of the picture while a shock front forms in the external medium in front of the disk.

is still efficient in stripping gas from the disk, but part of the removed material is now bound to the satellite by the dark halo gravity. The simulations were computed using three different resolutions, with m_h/h_{disk} equal to 2, 1 and 0.5. The stripped mass converges for $m_h/m_{disk} < 1$.

The dependence of ram pressure on the satellite orientation is not a simple function of the angle between the disk plane and the orbital velocity (Vollmer et al. 2001) and can depend on the ram pressure and the structure of the satellite (Abadi, Moore & Bower 1999; Quilis, Moore & Bower 2000; Schulz & Struck 2001; Marcolini, Brighenti & D’Ercole 2003). In the simulations E1 and E2 the galaxy is moving edge on through the hot gas. Comparing the amount of stripped mass of E1 and E2 with the results of the corresponding face on runs H2 and

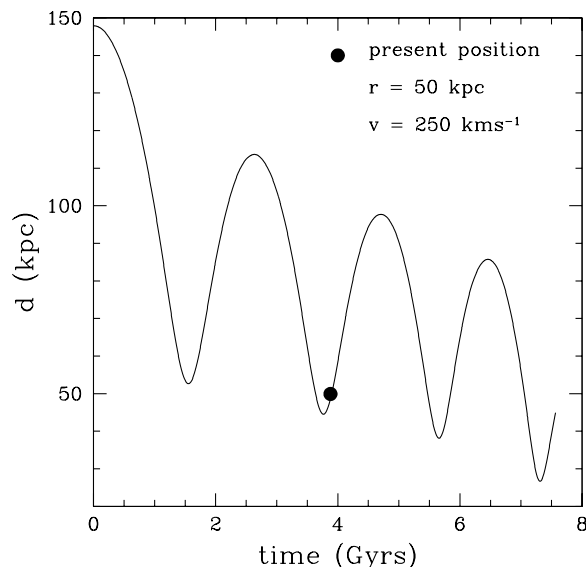


Figure 5. Orbital separation for the MW – LMC system

L1, it is clear that the stripping is not very sensitive to disk orientation. This implies that the amount of gas in the Stream will only slightly depend on the initial inclination of the LMC disk and on the precession eventually induced by tidal forces from the MW.

4 INTERACTING RUNS

4.1 Orbital parameters

The morphology of the Stream indicates that the orbit of the LMC is nearly polar and counter-clockwise, as seen from the Sun, while kinematical data (van der Marel et al. 2002) imply that the present position at ~ 50 kpc from the Galactic Center, is close to the perigalacticon. Since the mass ratio between the MW and its satellite is about 50:1, we expect that the effects of the dynamical friction are not negligible on time scales comparable with the orbital period. On the other hand, at each pericentric passage the LMC loses mass from tidal stripping, increasing its decay time: dynamical friction becomes less effective as the satellite approaches the Galaxy (Colpi, Mayer & Governato 1999).

Dynamical friction implies that we can not precisely make a backwards integration of the LMC’s orbit, therefore we make several low resolution test simulations (3×10^5 particles) in order to find the correct starting point for the LMC 4 Gyrs in the past such that it ends up with the present distance, velocity and orientation on the sky. We find orbital parameters close to the ones obtained by Gardiner, Sawa, & Fujimoto (1994) and Gardiner & Noguchi (1996). In particular the orbital plane is perpendicular to the Galactic disk, the present eccentricity (defined as $(r_{apo} - r_{per}) / (r_{apo} + r_{per})$, with r_{apo} and r_{per} apogalacticon and perigalacticon distances) and the orbital period are respectively 0.44 and ~ 2 Gyrs. The orbital separation between the MW and the LMC is plotted in Fig. 5 for the past 4 Gyrs and 4 Gyrs into the future. The satel-

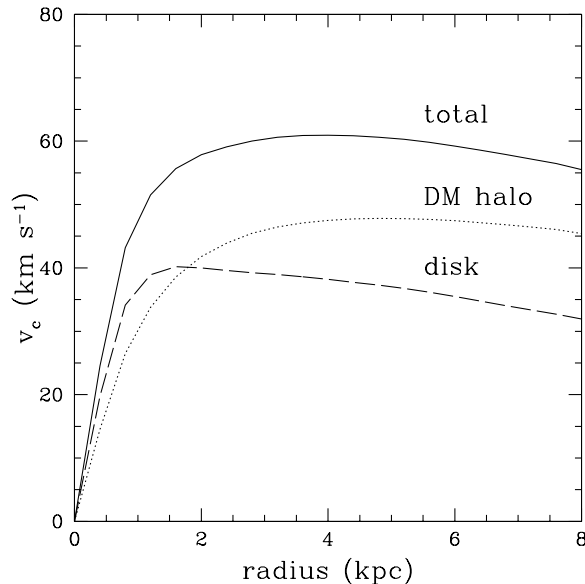


Figure 6. Final LMC rotation curve.

lite is currently at 50 kpc from the Galactic center and is moving away from the perigalacticon (at 45 kpc) with a velocity of 250 km s^{-1} . From the plot it appears evident that the orbit is slowly sinking, with each apogalactic distance $\sim 20\%$ smaller than the previous one. We will show in the next subsection that the change in the orbital parameters due to dynamical friction strongly affects the tidal forces and rate of ram pressure stripping.

In choosing the initial inclination and position of the line of nodes we make the approximation that they do not change during the interaction. In particular we adopt the values from van der Marel et al. (2002): respectively $i = 34.7^\circ$ and $\Theta = 129.9^\circ$. This choice could partially influence the final stellar structure of the disk, but not the ram pressure stripping process, as seen in the previous section.

4.2 The Stream

The close interaction with the MW strongly perturbs the entire structure of the satellite. In particular during the 4 Gyrs preceding the present epoch the LMC loses $\sim 80\%$ of its dark halo, and is currently tidally truncated at a radius of 11 kpc, consistent with the values provided by analytic calculations (Weinberg 2000; van der Marel et al. 2002) and with observations of the outer regions of the disk (Irwin 1991; van der Marel 2001). The contribution of the dark matter halo to the final rotation curve within 8 kpc from the center decreases by $\sim 5 \text{ km s}^{-1}$ and the disk component predominates in the inner region (Fig. 6).

While all the stars within the tidal radius are likely to be gravitationally bound, this is not true for gas. In fact, part of the gas that lies within the tidal radius can have enough thermal energy to escape from the potential well of the galaxy. Fig. 7 illustrates the evolution of the baryonic mass as function of time. The dotted and solid curve refers to the stellar and gaseous component respectively while the dashed curve represents the gas within the tidal radius which is actually bound to the LMC.

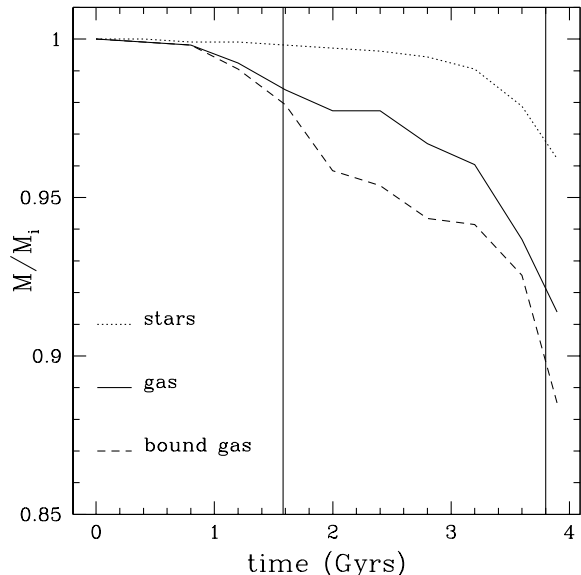


Figure 7. Fraction of stars and gas bound to the satellite during the last 4 Gyrs. Both the gas within the tidal radius and the bound gas are plotted. M_i is the initial mass of each disk component. The vertical solid lines indicate the perigalactica.

After two perigalactic passages the satellite loses roughly $\sim 12\%$ of its gas and $\sim 4\%$ of stars. A pure tidal stripping model would remove similar amounts of both stars and gas unless the initial gas disk was significantly more extended. The larger amount of stripped gas is due primarily to ram-pressure stripping: the rate at which gas is lost increases as the LMC approaches perigalacticon (the solid vertical lines in the plot), corresponding to higher densities of the diffuse halo gas and to higher velocities of the satellite along the orbit.

Stars are stripped from the LMC only during the last perigalacticon, since the previous perigalactic passage is too far from the MW to produce significant tidal shocks and to perturb the stellar structure of the satellite. The present stellar distribution (Fig. 8) indicates that a trailing and a small leading arm are forming (with surface density $\sim 3 \times 10^{-3} M_{\odot} \text{pc}^{-2}$), but most of the stars stripped from the disk are still bound to the LMC and form a large spheroidal component.

Contrary to the stars, gas is stripped during the first passage at perigalacticon, forming a continuous stream that lies in a thin plane (width ~ 25 kpc) perpendicular to the disk of the MW (Fig. 9) and between 50 and 75 kpc from the Galactic center. Our simulations predict that the MS forms a great circle, but most of the gas is lost recently and it is now at an angular distance between 10° and 120° from the LMC (comparable with the range provided by observations). The mass of the stripped gas ($1.4 \times 10^8 M_{\odot}$) is of the same order of magnitude as the observed amount of neutral hydrogen in the Stream by Putman et al. (2003a) ($2 \times 10^8 M_{\odot}$).

Fig. 10 represents the projection of the Stream as seen from an observer situated at the Galactic center who is looking toward the South Galactic Pole. The logarithmic colour scale indicates the column density gradient which gradually decreases along the length of the Stream. At a fixed distance

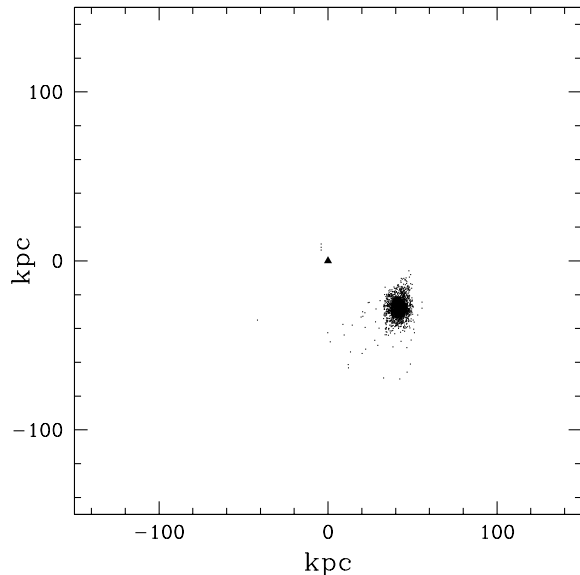


Figure 8. Present day distribution of stars from the LMC disk in a plane perpendicular to the Galactic plane.

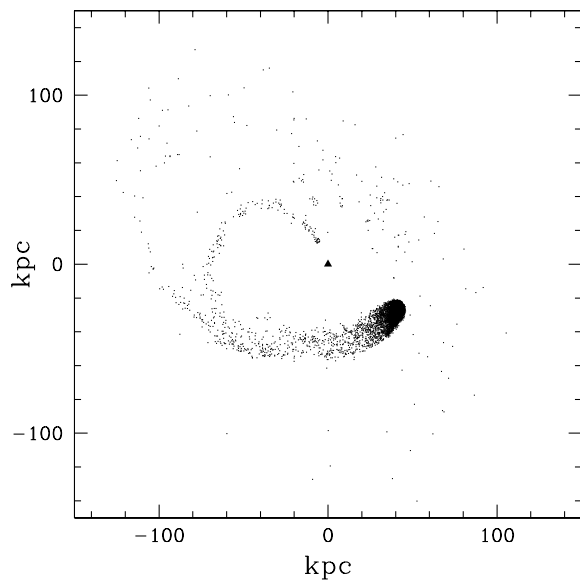


Figure 9. Final distribution of gas from the LMC disk in a plane perpendicular to the Galactic plane

from the LMC the structure of the Stream is not uniform but has clumpy and high density regions. The decrease in density is by nearly two orders of magnitude along the Stream (Fig. 11), due to the combination of two factors. The gas close to the head of the Stream is pulled from the disk during the last perigalacticon, when the stripping rate is maximum, whereas the tip is ~ 1 Gyr old and corresponds to an apogalactic passage. Moreover, the tail is formed by the first material stripped from the outer and low density regions of the exponential disk. This decrease in column density is a remarkable success for the ram-pressure scenario since tidal

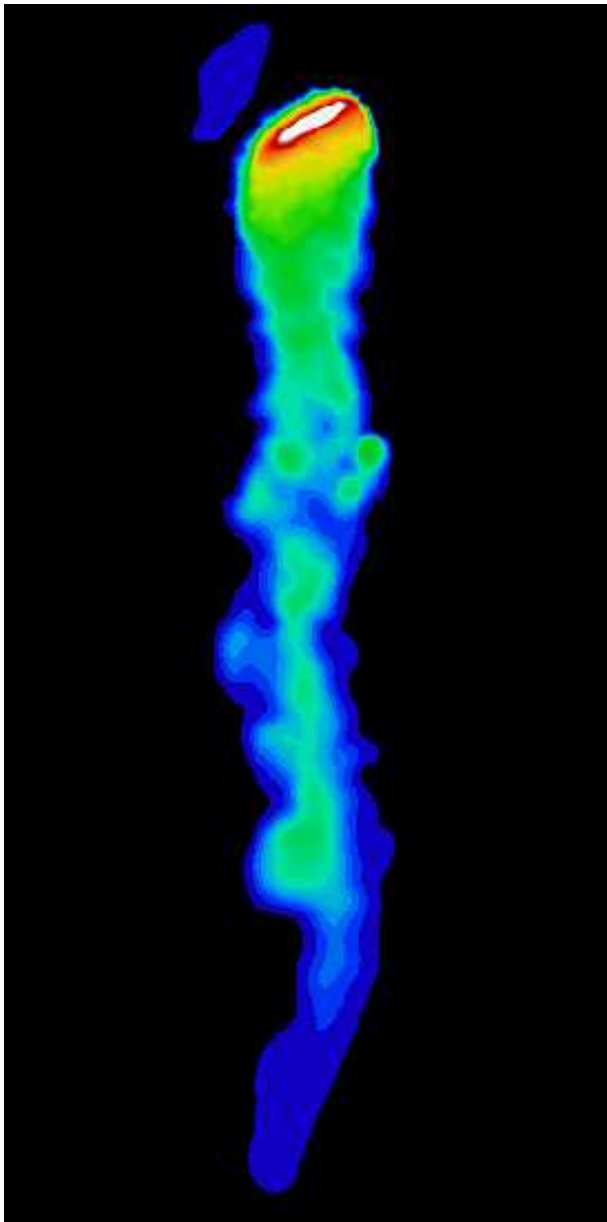


Figure 10. Hydrogen column density along the simulated stream. The intensity values are on a logarithmic scale with white corresponding to the highest density regions within the LMC disk and dark blue to $n_{\text{H}} \sim 10^{18} \text{cm}^{-2}$.

models generically produce streams with surface densities that fall off much more slowly.

The difference in the characteristic time scales of hydrodynamical and gravitational forces explains why a gaseous leading arm does not form through tidal stripping: gas is removed quite early from the outer regions of the LMC disk that during the second passage at the perigalacticon starts forming a leading arm feature. The great circle of stripped gas actually appears on the sky as a leading stream and could in principle reproduce observations of the leading arm (Fig. 9). This material was stripped from the satellite during the first orbit and is falling to the Galactic center in

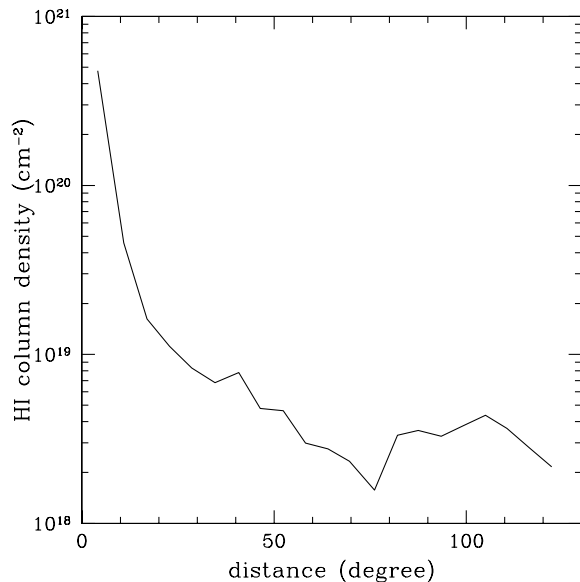


Figure 11. Hydrogen column density along the Stream. The system of coordinates is chosen in order to have the LMC at 0 degrees.

the Northern Galactic hemisphere, intersecting the actual position of the satellite.

The total amount of unbound gas after 4 Gyrs is comparable with the gas stripped in one orbital time from an LMC model in a test tube simulation with densities and velocities characteristic of a perigalactic passage. This means that the tidal forces acting on the satellite contribute to ram pressure processes: as a consequence of the resulting asymmetrical potential and distorted stellar disk, it is easier to strip more gas from the LMC's disk since the gravitational restoring force is weaker. Thus even a low density gaseous Galactic halo is able to remove a significant amount of gas from the LMC.

4.2.1 *Adiabatic versus cooling runs*

We have presented results from simulations that do not include radiative cooling. As discussed in section 3, in this case the gas in the disk of the LMC will increase its temperature as it is strongly compressed by the outer medium. In the adiabatic regime the gas can only lose energy by expansion, which requires a long timescale, and can become easily unbound due to this input of thermal energy. We have run a simulation with radiative cooling adopting a standard cooling function for primordial gas (hydrogen and helium). Since the gas quickly heats up to $\sim 10^5$ K, the peak of the cooling curve, then cools down on a timescale much shorter than the dynamical time, shrinking in radius compared to its original location. As a result a smaller gaseous disk results after a few cycles of heating and rapid cooling which sits deeper in the potential well and as a result no gas is stripped. However, what we are witnessing is probably the result of overcooling since we are neglecting the effect of star formation, namely heating from supernovae feedback and radiation from massive stellar associations. The LMC in particular shows widespread intense star formation across

its disk and bar. In reality a multi-phase ISM will result that will be eventually close to the condition of pressure equilibrium with the outer medium and will not be able to cool so efficiently. Until we can effectively model this multi-phase medium, we believe that the results of the adiabatic simulations are closer to reality.

4.3 The LMC disk

The Galactic disk remains unperturbed during the interaction, while the morphology of the satellite changes drastically. In particular we will focus on the changes in the stellar and gaseous structure of the LMC.

After 4 Gyrs from the beginning of the simulations almost the entire stellar component is still bound to the satellite, but less than 90% of the stars lies in the thin disk, which is surrounded by a stellar spheroid with a radius of ~ 11 kpc (Fig. 12). The structure of this spheroidal component is quite complex, since a strong warp that wraps 180° around the LMC is superimposed on the underlying low density stellar distribution. The warp forms after the first passage at the perigalacticon and involves a large fraction of the stellar particles. It extends up ~ 5 kpc out of the thin disk and is aligned with the major axis of the satellite. The existence of a warp is inferred by Kim et al. (1998) from the gas velocity field in the disk of the LMC, by van der Marel & Cioni (2001) and Olsen & Salyk (2002) using the apparent magnitude of different classes of stars as a distance indicator. The diffuse spheroidal component has an average surface density of $\sim 5 \times 10^{-2} M_\odot \text{pc}^{-2}$, which becomes one order of magnitude larger if we consider only the warp region. The warp deformation is partially directed along the line of sight and could have implications for the microlensing results, increasing the optical depth caused by self-lensing (Zaritsky & Lin 1997; Zhao & Evans 2000). The LMC's disk appears elongated, with a mean ellipticity $\epsilon = 0.38$ (where $\epsilon = 1 - q$ and q is the axial ratio), in a direction roughly aligned with the Galactic center and perpendicular to the Stream. These values agree very well with the observations provided by van der Marel (2001). Within the inner 6–7 kpc of the model LMC a strong and asymmetric bar forms after the first perigalacticon.

The isodensity contours of the face-on disk were fitted with ellipses using the MIDAS task FIT/ELL3. The ellipse centers, ellipticity and major axis position angle were considered as free parameters of the fitting procedure. The results of this projected analysis are illustrated in Fig. 13. The first plot on the top (solid line) shows the B-band surface brightness profile of the present face-on LMC, for which the best fitting exponential curve has a scale length of 1.5 kpc. The dashed line is the original exponential disk, with a scale length of ~ 1.7 kpc. The second and the third plot illustrate the variation of the position angle and eccentricity as a function of radius. The position angle is almost constant in the central 4 kpc of the disk and presents a sharp twist beyond this radius, which corresponds to the transition between the bar region and the outer density contours characterized by ellipticities $\lesssim 0.2$. At radii $\gtrsim 8$ kpc the disk appears more elongated, with a further increase in ellipticities and a twist of $\sim 50^\circ$ in the position angle. The last plot on the bottom indicates the drift of the countour centers in the plane of the

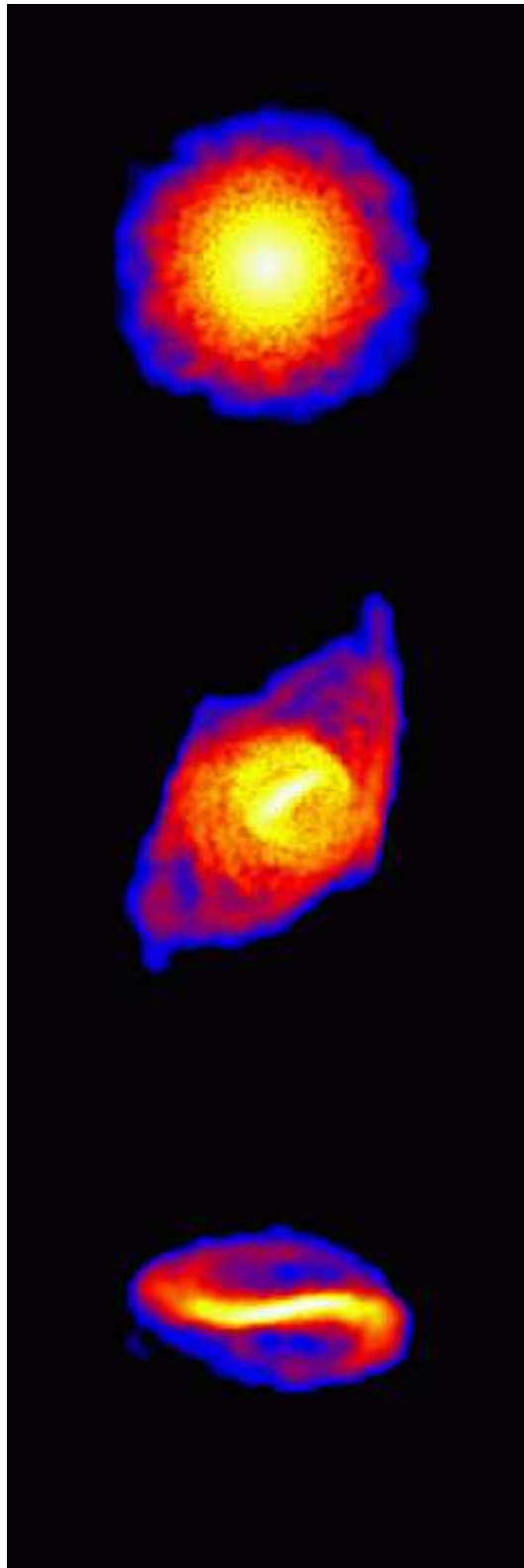


Figure 12. LMC stellar surface density. Colours represent a logarithmic scale where white corresponds to a density of $10^2 M_\odot \text{pc}^{-2}$ and blue to $10^{-2} M_\odot \text{pc}^{-2}$. From the top to the bottom: initial conditions, final face on and edge on projection. The bar and the strong warp are visible.

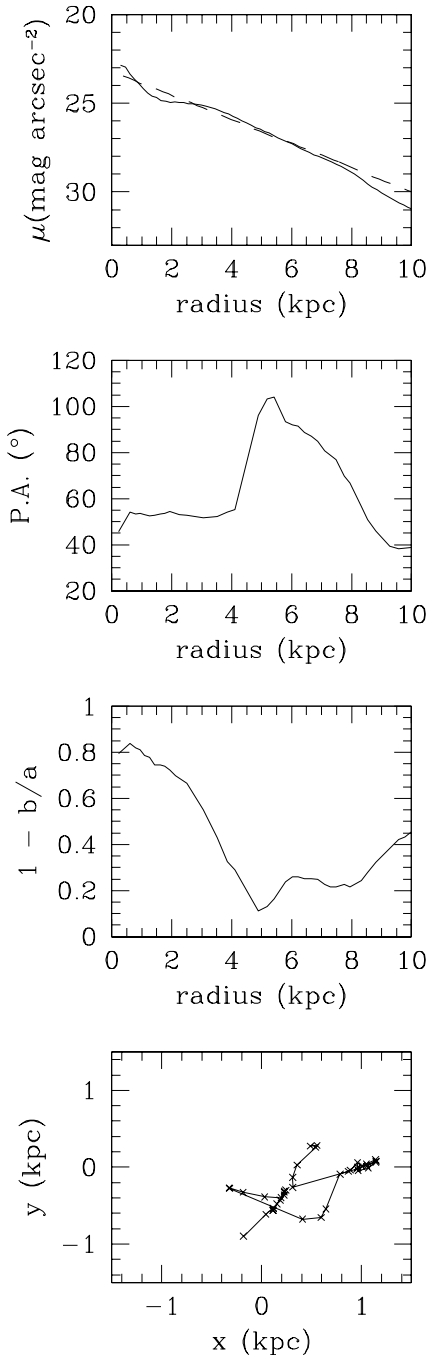


Figure 13. Photometric analysis of a face-on projection of the LMC disk. From the top to the bottom: B-band surface brightness, major axis position angle and ellipticity profiles. The last plot on the bottom represents the drift of the ellipse center in the plane of the disk.

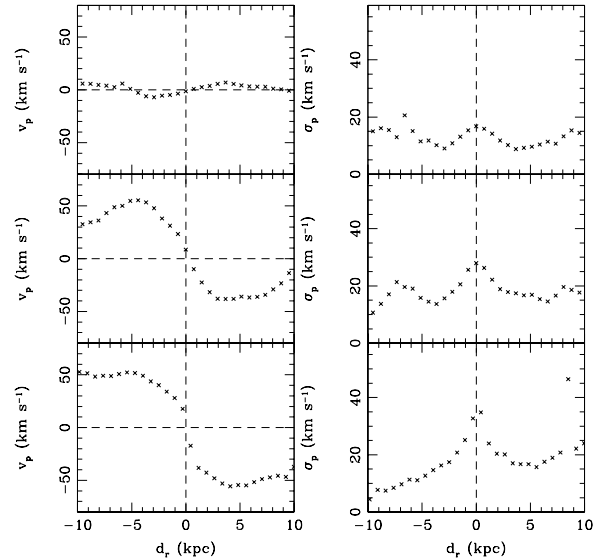


Figure 14. Projected velocity (left) and velocity dispersion (right) profiles for three different orientations of the LMC disk. From the top to the bottom: face-on, edge-on and end-on.

disk, which moves consistent with observations by almost 1 kpc.

Fig. 14 shows the kinematic profiles of three different orientations of the LMC disk observed today: from the top to the bottom face-on, edge-on and end-on projections. The peak in the velocity dispersion in the central 6–8 kpc is mainly due to the bar formation, while the external regions appear to be dominated by an hot tidally perturbed component with $\sigma_p \sim 20 \text{ km s}^{-1}$.

The gaseous disk is completely dominated by stripping processes (Fig 15). It retains a symmetric structure only within the central 12 kpc, in connection with the thin component of the stellar disk. Within this radius we do not observe a significant displacement between the center of the stellar distribution and the gaseous disk. The ram pressure stripping radius after 4 Gyrs is $\sim 6 \text{ kpc}$, a factor of three smaller than the initial disk radius and compatible with the results provided by HIPASS data (Putman, Gibson & Smith 1998).

5 CONCLUSIONS

We have carried out high resolution gravitational/hydrodynamical simulations of the interaction between the LMC and Milky Way. As the LMC spirals inwards towards the Galaxy it suffers ever increasing gravitational tidal forces and hydrodynamical stripping. Our simulations cover the previous 4 Gyrs of the orbit of the LMC such that at the final time it ends up at its correct location within the Galactic halo and with the observed inclination. We find that the combined effects of gravity and ram-pressure stripping can account for the majority of the LMC’s kinematical and morphological features and the morphology of Magellanic Stream.

Our model of the hot gaseous halo places a total of

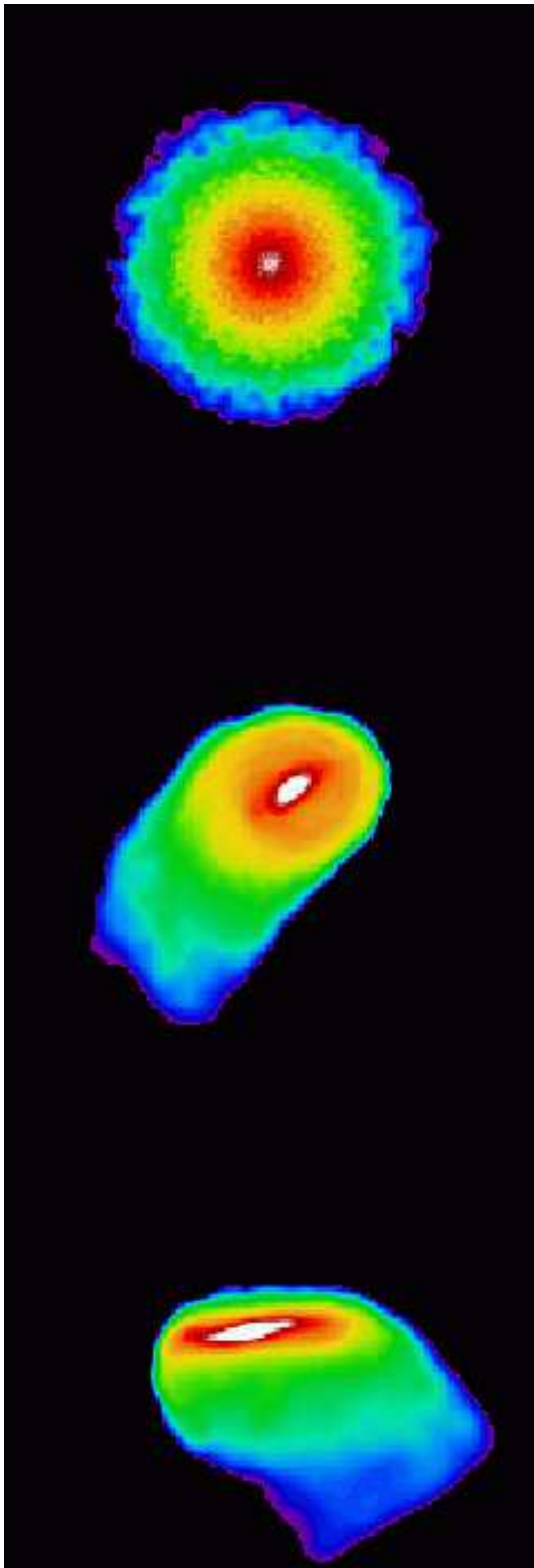


Figure 15. LMC gaseous column density. Colours represent a logarithmic scale where white corresponds to a density of 10^{22}cm^{-2} and violet to 10^{19}cm^{-2} . From the top to the bottom: initial conditions, final face on and edge on projection. The bar and the first part of the Stream are visible.

$10^9 M_{\odot}$ of ionised hydrogen within the dark matter halo of the Galaxy. The density at 50 kpc is $\approx 8 \times 10^{-5}$ atoms/cm³. This is sufficient to remove over $10^8 M_{\odot}$ of gas from the LMC, close to the observed mass of the Stream. The stripped gas forms a great circle, or a polar ring, around the Galaxy, consistently with the recently discovered extension of the Stream into the Northern Hemisphere by Braun & Thilker (2004). Less material was stripped during the pericentric passage 4 Gyrs ago since dynamical friction has moved the Clouds closer today. Thus we can reproduce the observed decrease in column density along the Stream. Very few stars are tidally removed from the LMC, but its disk becomes severely warped due to the tidal interaction. This creates a diffuse halo of stars within the LMC that may have been observed as self-lensing events. The disk of stars is elongated by 2:1 oriented towards the Galactic centre in agreement with the observations of van der Marel (2001).

Several improvements to our simulations could be made in order to study this fascinating interacting system in more detail. More detailed modelling of the star-formation and internal ISM of the LMC is necessary in order to study the role of gas stripping on star-formation, and the role of star-formation and the multiphase ISM on the stripping process. Including the interaction with the SMC which could supply a significant amount of gas to the Stream and may be responsible for the Magellanic bridge and the leading arm. Including a more realistic treatment of the gas physics in order to study the detailed structure of the stripped gas and its interaction with the halo gas as it infalls through the galactic halo.

REFERENCES

- Abadi, M. G., Moore, B., Bower, R. G. 1999, MNRAS, 308, 947
 Blitz, L., Robishaw, T. 2000, ApJ, 541, 675
 Braun, R., Thilker, D. A. 2004, A&A, 417, 421
 Brueck, M. T., Hawkins, M. R. S. 1983, A&A, 124, 216
 Colpi, M., Mayer, L., Governato, F. 1999, ApJ, 525, 720
 Cowie, L. L., McKee, C. F. 1977, ApJ, 211, 135
 Efstathiou, G., Lake, G., Negroponte, J. 1982, MNRAS, 199, 1069
 Fujita, Y. 2003, preprint (astro-ph 0311193)
 Gardiner, L. T., Sawa, T., Fujimoto, M. 1994, MNRAS, 266, 567
 Gardiner L. T., Noguchi M. 1996, MNRAS, 278, 191
 Guhathakurta, P., Reitzel, D. B. 1998, ASP Conf. Ser. 136: Galactic Halos, 22
 Gunn, J. E., Gott, J. R. I. 1972, ApJ, 176, 1
 Hernquist L. 1990, ApJ, 356, 359
 Hernquist L. 1993, ApJS, 86, 389
 Irwin, M. J. 1991, IAU Symp. 148: The Magellanic Clouds, 148, 453
 Kim S., Staveley-Smith L., Dopita M. A., Freeman K. C., Sault R. J., Kesteven M. J., McConnell D. 1998, ApJ, 503, 674
 Klypin A., Zhao H., Somerville R. S. 2002, ApJ, 573, 597
 Lin, D. N. C., Lynden-Bell, D. 1977, MNRAS, 181, 59
 Lin, D. N. C., Jones, B. F., Klemola, A. R. 1995, ApJ, 439, 652

- Majewski, S. R., Ostheimer, J. C., Kunkel, W. E., Johnston, K. V., Patterson, R. J., Palma, C. 1999, IAU Symp. 190: New Views of the Magellanic Clouds, 190, 508
- Marcolini A., Brighenti F., D'Ercole A. 2003, preprint (astro-ph 0309026)
- Mathewson, D. S., Ford, V. L., Schwarz, M. P., Murray, J. D. 1979, IAU Symp. 84: The Large-Scale Characteristics of the Galaxy, 84, 547
- Mathewson, D. S., Wayte, S. R., Ford, V. L., Ruan, K. 1987, Proceedings of the Astronomical Society of Australia, 7, 19
- Mayer, L., Wadsley, J. 2004, MNRAS, 347, 277
- Meurer, G. R., Bicknell, G. V., Gingold, R. A. 1985, Proceedings of the Astronomical Society of Australia, 6, 195
- Mo, H. J., Mao, S., White, S. D. M. 1998, MNRAS, 295, 319
- Moore, B., Davis, M. 1994, MNRAS, 270, 209
- Mori, M., Burkert, A. 2000, ApJ, 538, 559
- Murai, T., Fujimoto, M. 1980, PASJ, 32, 581
- Murali, C. 2000, ApJL, 529, L81
- Murray, S. D., White, S. D. M., Blondin, J. M., Lin, D. N. C. 1993, ApJ, 407, 588
- Navarro J. F., Frenk C. S., White S. D. M. 1996, ApJ, 462, 563
- Navarro J. F., Frenk C. S., White S. D. M. 1997, ApJ, 490, 493
- Nulsen, P. E. J. 1982, MNRAS, 198, 1007
- Olsen, K. A. G., Salyk, C. 2002, AJ, 124, 2045
- Putman, M. E., Gibson, B., K., Staveley-Smith, L. 1998 IAU Symp.190, New Views of the Magellanic Clouds, eds. Chu et al.
- Putman, M. E. et al. 1998, Nat, 394, 752
- Putman, M. E., Staveley-Smith, L., Freeman, K. C., Gibson, B. K., Barnes, D. G. 2003, ApJ, 586, 170
- Putman, M. E., Bland-Hawthorn, J., Veilleux, S., Gibson, B. K., Freeman, K. C., Maloney, P. R. 2003, ApJ, 597, 948
- Quilis, V., Moore, B., Bower, R. 2000, Science, 288, 1617
- Quilis, V., Moore, B. 2001, ApJL, 555, L95
- Sarazin, C. L. 1986, Reviews of Modern Physics, 58, 1
- Schulz, S., Struck, C. 2001, MNRAS, 328, 185
- Sembach, K. R. 2003, preprint (astro-ph 0311089)
- Sembach, K. R. et al. 2003, ApJS, 146, 165
- Sofue, Y. 1994, PASJ, 46, 431
- Springel V., White S. D. M. 1999, MNRAS, 307, 162
- Stanimirovic, S., Dickey, J. M., Krčo, M., Brooks, A., M. 2002, ApJ, 576, 773
- Taffoni, G., Mayer, L., Colpi, M., Governato, F. 2003, MNRAS, 341, 434
- Toomre, A. 1964, ApJ, 139, 1217
- Toomre, A. 1981, in The structure and evolution of normal galaxies, Cambridge University Press, 1981, p. 11
- van der Marel, R. P. 2001, AJ, 122, 1827
- van der Marel, R. P., Cioni, M. L. 2001, AJ, 122, 1807
- van der Marel R. P., Alves D. R., Hardy E., Suntzeff N. B. 2002, AJ, 124, 2639
- Vollmer, B., Cayatte, V., Balkowski, C., Duschl, W. J. 2001, ApJ, 561, 708
- Wadsley, J. W., Stadel, J., Quinn, T. 2004, New Astronomy, 9, 137
- Weinberg, M. D. 1995, ApJL, 455, L31
- Weinberg, M. D. 1998, MNRAS, 299, 499
- Weinberg, M. D. 2000, ApJ, 532, 922
- Weiner, B. J., Williams, T. B. 1996, AJ, 111, 1156
- White, S. D. M., Frenk, C. S. 1991, ApJ, 379, 52
- Zaritsky, D., Lin, D. N. C. 1997, AJ, 114, 2545
- Zhao, H., Evans, N. W. 2000, ApJL, 545, L35